FULL PAPER

Rational Design of Small Molecular Donor for Solution-Processed Organic Photovoltaics with 8.1% Efficiency and High Fill Factor via Multiple Fluorine Substituents and Thiophene Bridge

Jin-Liang Wang, Qing-Ru Yin, Jing-Sheng Miao, Zhuo Wu, Zheng-Feng Chang, Yue Cao, Ru-Bo Zhang,* Jie-Yu Wang,* Hong-Bin Wu,* and Yong Cao*

A series of tetrafluorine-substituted small molecules with a D_1-A-D_2-A-D_1 linear framework based on indacenodithiophene and difluorobenzothiadiazole is designed and synthesized for application as donor materials in solution-processed small-molecule organic solar cells. The impacts of thiophene π-bridge and multiple fluorinated modules on the photophysical properties, the energy levels of the highest occupied molecular orbitals (HOMO) and lowest unoccupied molecular orbitals (LUMO), charge carrier mobility, the morphologies of blend films, and their photovoltaic properties as electron donor material in the photoactive layer are investigated. By incorporating multiple fluorine substituents of benzothiadiazole and inserting two thiophene spacers, the fill factor (*FF*), open-circuit voltage, and short-circuit current density are dramatically improved in comparison with fluorinated-free materials. With the solvent vapor annealing treatment, further enhancement in charge carrier mobility and power conversion efficiency (PCE) are achieved. Finally, a high PCE of 8.1% with very-high *FF* of 0.76 for BIT-4F-T/$PC_{71}BM$ is achieved without additional additive, which is among one of the highest reported for small-molecules-based solar cells with PCE over 8%. The results reported here clearly indicate that high PCE in solar cells based small molecules can be significantly increased through careful engineering of the molecular structure and optimization on the morphology of blend films by solvent vapor annealing.

1. Introduction

Solution-processed bulk-heterojunction organic solar cells (BHJ-OSCs) have attracted considerable attention as a promising renewable energy resource because of their low mass, flexibility, and potentially inexpensive manufacturing in recent years.[1] The development of donor/acceptor materials device architectures has led to record power conversion efficiencies (PCEs) of ≈10% for soluble π-conjugated polymers in single-junction solar cells.[2] However, the polydispersity of polymers can represent these problems such as the reproducibility of the synthesis, purification, and electronic properties of the final active materials. Over the past few years, solution-processed small-molecules BHJ-OSCs have been investigated as an attractive alternative to polymeric counterparts as a donor component in fullerene-based BHJ-OSCs.[3] They possess several impressive advantages such as monodisperse and well-defined structures, ease of purification, no end-group contaminants, and

Prof. J.-L. Wang, Dr. Q.-R. Yin, Dr. Z. Wu, Dr. Z.-F. Chang, Prof. R.-B. Zhang
Beijing Key Laboratory of Photoelectronic/Electrophotonic Conversion Materials
Key Laboratory of Cluster Science of Ministry of Education
School of Chemistry
Beijing Institute of Technology
5 South Zhongguancun Street, Beijing 100081, China
E-mail: jinlwang@bit.edu.cn; zhangrubo@bit.edu.cn

Dr. J.-S. Miao, Prof. H.-B. Wu, Prof. Y. Cao
Institute of Polymer Optoelectronic Materials and Devices
State Key Laboratory of Luminescent Materials and Devices
South China University of Technology
381 Wushan Road, Guangzhou 510640, China
E-mail: hbwu@scut.edu.cn

Dr. Y. Cao, Dr. J.-Y. Wang
The Key Laboratories of Bioorganic Chemistry and Molecular Engineering of Ministry of Education
College of Chemistry and Molecular Engineering
Peking University
Beijing 100871, China
E-mail: jieyuwang@pku.edu.cn

DOI: 10.1002/adfm.201500190

superior batch-to-batch reproducible performance compared to polymer counterparts. Moreover, another advantage of small molecules is that they provide more reliable analyses of structure–properties–device performance relationships and disclose the key of the design of high performance photovoltaic materials. Therefore, the performance of solution-processed BHJ-OSCs based on small molecules has been dramatically increased over the past few years, which is approaching the record of polymer solar cells.[4] To date, state-of-the-art solution-processed small-molecules single-junction BHJ-OSCs based on benzodithiophene (BDT) core by Chen's group have exhibited best PCEs of ≈9.9% after the optimizations of molecular structures and device conditions in comparison with the first reported PCE of 5.4%.[5] Meanwhile, Bazan and Heeger's groups have reported the synthesis of small molecules based on dithienosilole (DTS) core unit and the best devices showed a PCE of around 8.9% after the optimizations of molecular structures and in conjunction with ZnO optical spacer, which is a significant progress when compared with its initial PCE of 6.7%.[6] However, there are no other building blocks-based small-molecule donor materials with over 8% efficiency reported up to date. To enrich the pool of high-performance small-molecule donor materials and reduce the gap between the small-molecules-based BHJ-OSCs and their polymer counterparts, the most straightforward and effective approaches are new molecular design, optimization on the morphology of blend films, and device engineering to in-depth understand the design principle of such donor materials.

Although attachment of fluorine substituent has been proven to be a useful strategy to tune the optical and electronic properties of conjugated materials,[7] it remains a difficult task when incorporating multiple fluorine substituents ($n > 2$) in a single small molecule for highly efficient photovoltaic materials. Meanwhile, indacenodithiophene (IDT) unit has been attracting considerable attention in organic field-effect transistors (OFETs) and BHJ-OSCs due to its rigid and coplanar heteroaromatic ladder-type structure.[8] However, to the best of our knowledge, small molecules based on the IDT unit and difluorinated benzothiadiazole as building blocks have never been reported to date mainly due to less solubility of target materials. More importantly, compared with the high regiochemistry of monofluorinated benzothiadiazole for coupling reaction,[6c] it is very challenging to highly synthesize the targeted molecules due to lack of an appropriate method to afford mono-functionalized difluorinated benzothiadiazole in high isolated yield.

To address this challenge, we design and synthesize a series of multifluorine substituted small molecules based on D_1-A-D_2-A-D_1 linear frameworks and investigate the effects of π-bridge unit and multiple fluorinated modules on the photophysical properties, the HOMO/LUMO energy level, charge carrier mobility, the morphologies of blend films, and their photovoltaic properties as electron donor material in the photoactive layer. As shown in **Figure 1**, all of the target molecules have an IDT-based core as the central donor unit (D_2), with two benzothiadiazole or difluorobenzothiadiazole as the acceptor (A), and two *n*-hexyl-substituted bithiophene as the terminal donor groups (D_1). Benzothiadiazole unit often has flanking thiophenes (i.e., DTBT) when being used as an acceptor in D–A copolymers; therefore, it was desirable

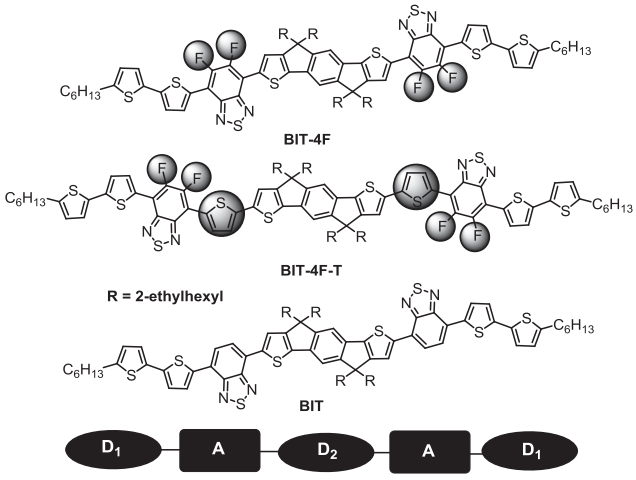

Figure 1. Chemical structures of **BIT-4F**, **BIT-4F-T**, and **BIT**.

to employ an extra thiophene π bridge unit in **BIT-4F-T** to a) enhance the light-harvesting ability of the whole molecule; b) improve molecular planarity and enhance π-electron delocalization and solid-state intermolecular packing; and (c) keep relatively deep HOMO energy levels and give high open-circuit voltage (V_{oc}). These materials both exhibit good solubility in common organic solvents such as $CHCl_3$, THF, and toluene owing to the four 2-ethylhexyls and two hexyls, and thus can readily be solution-processed and form excellent smooth films by spin-coating. In combination with using $PC_{71}BM$ as the acceptor, the BHJ-OSC devices based on **BIT-4F-T**, which shows a more extended conjugated length than that of **BIT-4F**, exhibited PCE of 8.1%, with a high V_{oc} of 0.90 V, short-circuit current density (J_{sc}) of 11.9 mA cm^{-2}, and a very-high *FF* of 0.76 for the device without using any additives. To the best of our knowledge, this is the highest PCE of solution-processed BHJ solar cells based on IDT units small molecules reported to date, and is among one of the best small-molecule donor materials in single-junction solar cells. Surprisingly, the device based on similar chemical structures **BIT** or **BIT-4F** and **$PC_{71}BM$** gives much lower PCEs, respectively. The reason that is responsible for the difference is, therefore, of intense research interest and investigated thoroughly in this study to unveil the relevant structure–property–performance relationships of these D_1-A-D_2-A-D_1 linear small molecules.

2. Results and Discussion

The synthetic routes to these D_1-A-D_2-A-D_1 linear small molecules are shown in **Scheme 1**. Four 2-ethylhexyl chains were installed into IDT (**1**)[9] under base condition and KI as the catalyst to obtain **2** in 75% isolated yield. Treatment of **2** with *n*-BuLi followed by trimethyltin chloride facilely gave the ditin reagent **3** as light-yellow oil that was directly used in the next step without any further purification. **4** was prepared through the Stille coupling reactions between **3** and 2-bromothiophene using a $Pd_2(dba)_3$/P(*o*-tolyl)$_3$ catalytic system in 85% isolated yield. Then, **4** can be lithiated by *n*-BuLi followed by quenching with trimethyltin chloride to afford extended ditin reagent **5**.

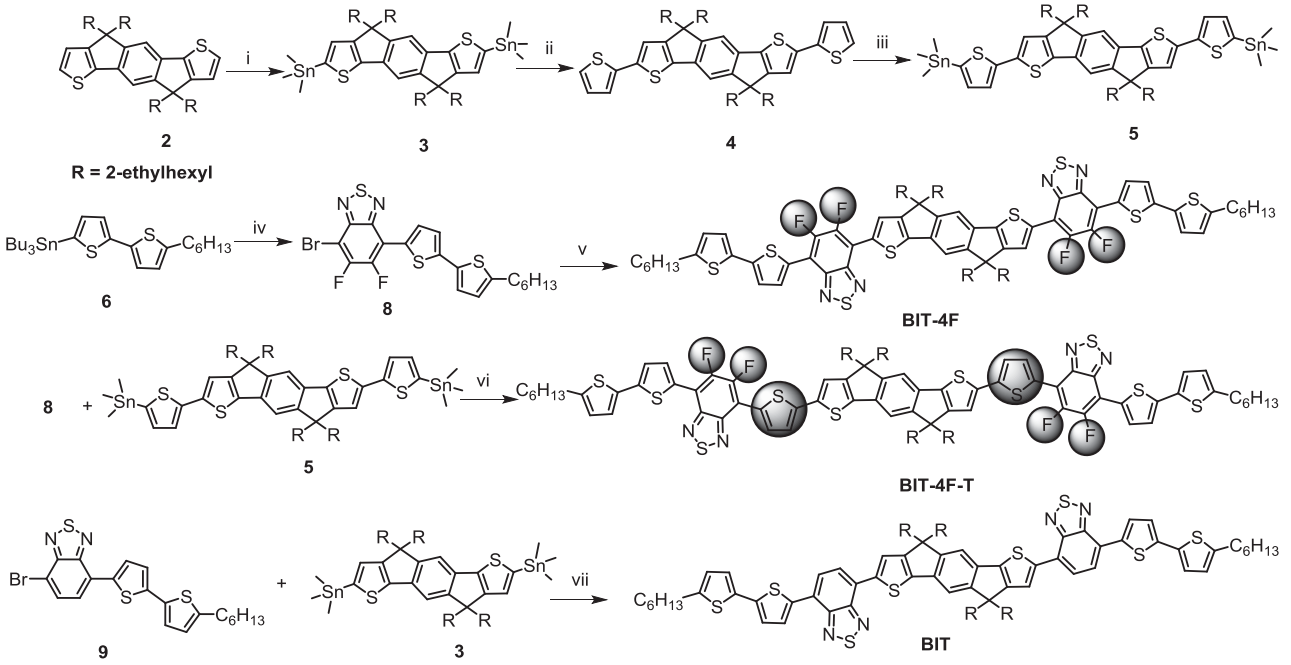

Scheme 1. Synthesis of **BIT-4F**, **BIT-4F-T**, and **BIT**. Reagents and conditions: (i) a) *n*-BuLi, THF, −78 °C, 1 h. b) $(CH_3)_3SnCl$, THF, −78 °C to rt, 10 h, 97%; ii) $Pd_2(dba)_3$, P(*o*-tolyl)$_3$, 2-bromothiophene, toluene, reflux, 12 h, 85%; (iii) a) *n*-BuLi, THF, −78 °C, 1 h. b) THF, $(CH_3)_3SnCl$, −78 °C to rt, 10 h, 98%; (iv) 4,7-dibromo-5,6-difluorobenzo[c][1,2,5]thiadiazole (**7**), $Pd_2(dba)_3$, P(*o*-tolyl)$_3$, toluene, rt, 12 h, 32%; (v) **3**, $Pd_2(dba)_3$, P(*o*-tolyl)$_3$, Toluene, reflux, 12 h, 86%; (vi) $Pd_2(dba)_3$, P(*o*-tolyl)$_3$, Toluene, reflux, 12 h, 61%; (vii) $Pd_2(dba)_3$, P(*o*-tolyl)$_3$, Toluene, reflux, 12 h, 91%.

The important monobromide intermediate **8** was prepared by monotin reagents **6**[10] and **7**[11] in 32% isolated yield. **BIT-4F** and **BIT-4F-T** were obtained through a twofold Stille coupling reaction between **8** and ditin **3** or **5** as dark solid in 86% and 61% isolated yield, respectively. Meanwhile, **BIT** was synthesized between **9**[12] and ditin **3** as a dark solid in 91% isolated yield. All compounds were purified by silica gel column chromatography, and their structures and purity were verified by ^1H and ^{13}C NMR, elemental analysis, and Electrospray Ionization (ESI)/Matrix-Assisted Laser Desorption ionization Time-of-flight (MALDI-TOF) MS. The thermal property of these small molecules was investigated by thermogravimetric analysis (TGA) (Figure S1, Supporting Information). Under N_2 atmosphere, the onset temperature with 5% weight loss is about 414 °C for **BIT**, 413 °C for **BIT-4F**, and 405 °C for **BIT-4F-T**, respectively, which indicated that the thermal stability of these molecules is adequate for application in organic solar cells.

To investigate the relationship between the molecular structure and the photophysical property, the absorption spectra of these small molecules both in diluted chloroform solutions and in thin films obtained by spin-coating are recorded in **Figure 2**. All molecules showed two distinct absorption bands (Band I: 300–450 nm; Band II: 450–700 nm) in solution and solid state due to π–π^* transition of conjugated backbone for Band I and the intramolecular charge transfer (ICT) between the molecular donor and the acceptor unit Band II. In solution, introduction of fluorine atoms in **BIT-4F** exhibited a noticeable blue-shift by 13 nm at λ_{max} and slight increases of the molar

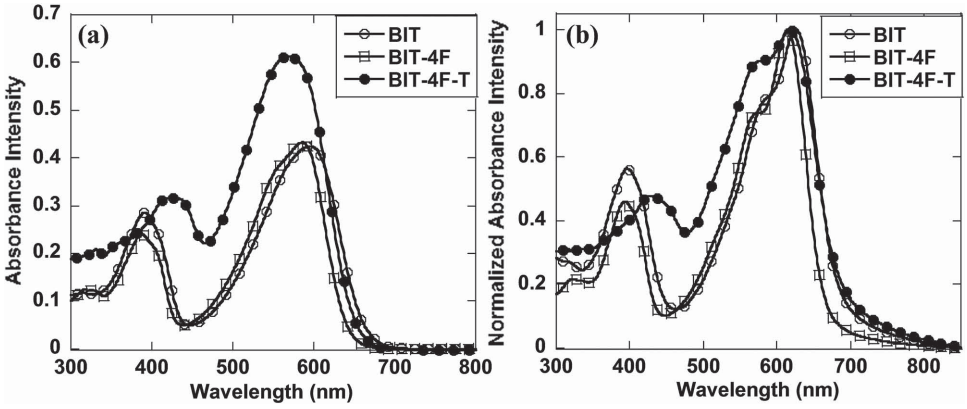

Figure 2. The absorption spectra of these D_1-A-D_2-A-D_1 linear small molecules (a) in chloroform solutions (5×10^{-6} m) and (b) in the thin films.

Table 1. Photophysical and electrochemical properties of D_1-A-D_2-A-D_1 small molecules in solutions and the thin films.

Compd.	λ_{max}abs. (sol) [nm] (log ε)	λ_{max}abs. (film) [nm]	$E_{ox(onset)}$ [V]	$E_{red(onset)}$ [V]	E_{HOMO} [eV]	E_{LUMO} [eV]	$E_{g(cv)}$ [eV]	$E_{g(opt)}$ [b] [eV]
BIT	390 (4.70), 595 (4.91)	394, 580, 626	0.51[a]	−1.56[a]	−5.31	−3.24	2.07	1.77
BIT-4F	386(4.75), 586 (4.92)	392, 567, 614	0.68[a]	−1.48[a]	−5.48	−3.32	2.16	1.83
BIT-4F-T	420(4.81), 569 (5.09)	426, 575, 618	0.53[a]	−1.53[a]	−5.33	−3.27	2.06	1.76

[a]Potentials are measured relative to a F_c/F_c^+ redox couple as an external reference; [b]Estimated from the onset of thin-film absorption.

extinction coefficient values (ε) of λ_{max} in comparison with **BIT**. Moreover, obvious shoulder features are shown in **BIT-4F**, which might be attributed to the increase of molecular rigidity and planarity through the fluorine–sulfur or fluorine–hydrogen interactions between benzothiadiazole and IDT units. Although the molar extinction coefficient of the absorption peaks in **BIT-4F-T** increased obviously relative to these of **BIT-4F** by inserting two thiophene units between IDT and difluorobenzothiadiazole units, the maximum absorption peak (λ_{max}) in band II of **BIT-4F-T** caused dramatically blueshift by 17 nm. In contrast, the absorption spectra of these D_1-A-D_2-A-D_1 small molecules in films are redshifted and increased the relative intensity of their 0–0 vibrational peak. Such features are attributed to a higher π-electron delocalization and more planar conjugated backbone in the solid state. Compared with those absorption maxima in solutions, **BIT** and **BIT-4F** showed redshift of 31 and 28 nm, respectively, whereas the thin films of **BIT-4F-T** display the largest redshift of 49 nm on the maximum absorption peak (λ_{max}) and most obvious shoulder peaks relative to these solutions. These results are probably due to the bigger conformation change, more efficient interchain interaction, and the higher π-electron delocalization of **BIT-4F-T** in the solid states, which could be beneficial to a higher hole mobility. From the onset of absorption, the optical band gaps of the films were estimated to be 1.77 eV for **BIT**, 1.83 eV for **BIT-4F**, and 1.76 eV for **BIT-4F-T**, respectively, as listed in **Table 1**. Moreover, these small molecules were nonluminescent in thin films due to efficient interchain interaction and feature of ICT in the solid state. It is clear that **BIT-4F-T** has the strongest absorption bands among these three materials and that is preferable to high photovoltaic performance for BHJ solar cells as discussed below.

In order to investigate the relationship between the chemical structures and the electrochemical properties of the desired materials, the cyclic voltammetry (CV) experiments of these three materials in thin films were conducted. The CV curves of these compounds showed one quasi-reversible p-doping process and n-doping process (Figure S2, Supporting Information). The HOMO and LUMO levels are −5.31 eV/−3.24 eV for **BIT**, −5.48 eV/−3.32 eV for **BIT-4F**, and −5.33 eV/−3.27 eV for **BIT-4F-T**, respectively, according to the following equation of $E_{HOMO} = -e(E_{ox} + 4.80)$ (eV) and $E_{LUMO} = -e(E_{red} + 4.80)$ (eV). **BIT-4F** showed obvious deeper HOMO levels (ΔE = 0.17 eV) relative to **BIT** due to the electronic withdrawing nature of four fluorine groups on the two benzothiadiazole.[13] In contrast, changes in LUMO energy levels on fluorine substitution are less notable, which result in an increase of the band gap of **BIT-4F**. The HOMO and LUMO energy levels of **BIT-4F-T** are similar to those of **BIT**, although they are upshifted in comparison with those of **BIT-4F** due to the electron-donating effect of the thiophene bridge. The electrochemical band gaps ($E_{g(cv)}$) are albeit slightly larger than the corresponding optical band gaps ($E_{g(opt)}$) due to different measurement methods. Such deep-lying HOMO energy levels are expected to high V_{oc} of the resultant organic solar cells.

To understand the microinfluence of fluorination and thiophene spacers on both the backbone conformation and physical properties of desired materials, the geometries of these small molecules were optimized with the DFT B3LYP/6-31G(d) method.[14] Each compound has two local minimum energy conformations due to "*trans*" or "*cis*" conformation of the two flanking thiophene with BT unit, namely linear and curved conformations, respectively (Figure S3, Supporting Information). These two conformations of each compound have almost the equal Gibbs free energy, and the curved conformation was slightly lower energy than its counterpart, which is consistent with the previous literature.[8d] As compared with the conformation of **BIT**, the two local minimum conformations of **BIT-4F** exhibited obviously more co-planar between difluorinated BT and its flanking thiophene units, particularly for linear conformation. According to the previous literature,[8d] the improvement of the local co-planarity around the BT units should be attributed to the noncovalent interaction between F and S and/or F and H atoms. Moreover, compared with **BIT** and **BIT-4F**, the perfect co-planarity local energy minimum conformations were slightly damaged in the curved conformation of **BIT-4F-T** due to a slight twist between the inserting thiophene spacer and IDT units. The difluorinated BT units can strongly decrease HOMO level. For example, the decreased HOMO value of **BIT-4F** is ≈0.12–0.14 eV in comparison with **BIT** based on the DFT B3LYP/6-31G(d) method (Figure S4, Supporting Information). Considerations to the complex effects from both additions of thiophene spacer and fluorinated substitution, the largest difference of both HOMO and LUMO levels occurs in **BIT-4F-T** based on DFT, which is consistent with the blueshift of the maximum absorption peak in a diluted solution. Additional thiophene unit contributes to decrease of the first excited energies but dramatical increase of their oscillator strength, which means increase of molar extinction coefficient of **BIT-4F-T**. The replacement of BT with difluorinated BT can slightly increase the first excited energies and their oscillator strength. In addition, thiophene spacer can, as expected, increase transition dipole moments. According to the excitation energies, dipole moments of the molecules in both ground and excited states and transition dipole moments could be estimated and as shown in Table S1 (Supporting Information). These results show that **BIT-4F-T** has biggest dipole moment change from the ground to the first exited state, which contributed to high

Table 2. A summary of the device performances of the organic solar cells from the D_1-A-D_2-A-D_1 small molecules.

Active layer	Ratio [w/w]	J_{sc} [mA cm^{-2}]	V_{oc} [V]	*FF* [%]	PCE [%]
BIT/PC$_{71}$BM	1:3	7.2	0.90	38	2.5
BIT-4F/PC$_{71}$BM	1:3	8.6	0.99	36	3.1
BIT-4F/PC$_{71}$BM	1:2	9.0	0.99	38	3.4
BIT-4F-T/PC$_{71}$BM	1:3	11.4	0.94	60	6.5
BIT-4F-T/PC$_{71}$BM	1:4	10.3	0.95	56	5.5
BIT-4F-T/PC$_{71}$BM	1:2	11.7	0.94	62	6.8
BIT-4F-T/PC$_{71}$BM	1:1.5	9.7	0.94	59	5.4
BIT-4F-T/PC$_{71}$BM[a)]	1:2	11.9	0.90	76	8.1
BIT-4F-T/PC$_{71}$BM[b)]	1:2	11.1	0.89	75	7.4
BIT-4F-T/PC$_{71}$BM[a)]	1:3	11.1	0.89	74	7.3
BIT-4F-T/PC$_{71}$BM[b)]	1:3	10.8	0.90	72	7.0

[a)]Treatment with CH_2Cl_2 vapor annealing for 30 s; [b)]Treatment with CH_2Cl_2 vapor annealing for 50 s.

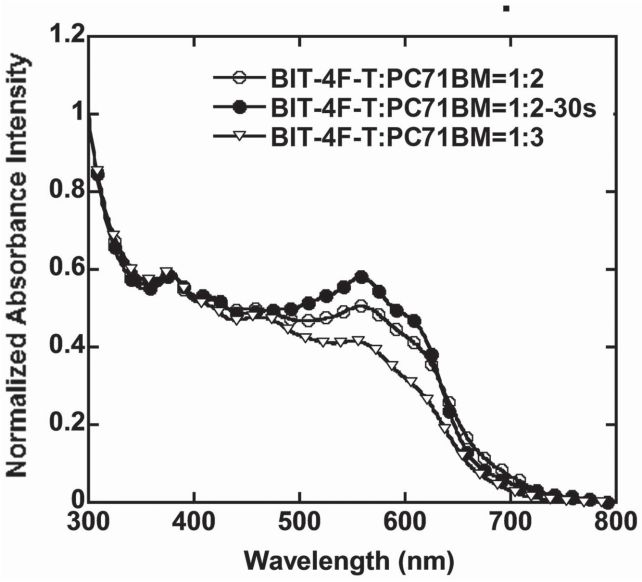

Figure 3. Absorption spectra of **BIT-4F-T:**PC$_{71}$BM (1:2 and 1:3, w/w) blend films and the film (1:2) after treatment with CH_2Cl_2 vapor annealing.

photovoltaic performance for BHJ solar cells as discussed below.

To demonstrate the potential of these D_1-A-D_2-A-D_1 small molecules as promising electron donor materials in organic solar cells, we fabricated BHJ-OSCs with a device structure ITO/PEDOT:PSS/small molecule donor: **PC$_{61}$BM** (or **PC$_{71}$BM**)/PFN/Al,[15] with a preliminary D/A ratio of 1:3. The optimized thicknesses of the active layers were determined to be 90–100 nm. **Table 2** and Table S2 (Supporting Information) summarize the device performance, such as V_{oc}, J_{sc}, *FF*, and PCE of the devices under 1 sun illumination. As expected, all of the devices based on our three small molecules exhibited high V_{oc} (≥0.89 V) due to the relative lower lying HOMO energy levels of donor materials, especially for **BIT-4F** with PC$_{61}$BM being about 0.99 V. By replacing PC$_{61}$BM with PC$_{71}$BM as the acceptor, the PCEs are 2.5% (**BIT**), 3.1% (**BIT-4F**), 6.5% (**BIT-4F-T**), respectively, at 1:3 weight ratios between donor and **PC$_{71}$BM**. The significantly improved PCE in **BIT-4F-T** devices are mainly due to their higher *FF* of 0.60 and higher J_{sc} of 11.4 mA cm^{-2}, when in comparison with other two donor materials. Indeed, our strategy of inserting thiophene π bridge units and multiple fluorine substituents in **BIT-4F-T** is very effective and successful in enhancing J_{sc} and FF without sacrificing the V_{oc} despite its lowest bandgap.

In order to further optimize the device performance, the effect of different **BIT-4F-T**: PCBM ratios (D:A = 1:4, 1:2, 1:1.5, w/w) on device performance was also investigated systematically. Optimal performance was obtained when the weight ratio of **BIT-4F-T: PC$_{71}$BM** is 1:2, resulting in a J_{sc} = 11.7 mA cm^{-2}, V_{oc} = 0.94 V, *FF* =62%, and PCE = 6.8%. The substantial J_{sc} improvement (11.7 mA cm^{-2} vs 9.7 mA cm^{-2}) upon the change of blend ratio can partially be attributed to stronger optical absorption coverage in whole visible region, which can clearly be seen from **Figure 3**. Indeed, the blend film with a 1:2 ratio of donor/PC$_{71}$BM showed an obvious enhancement in absorption spectra in the range of 450–750 nm when compared with the film from the 1:3 blend.

As an effective method for enhancement of PCE, solvent vapor annealing has been used in BHJ-OSCs to optimize the morphology of the active layer.[16] We further optimize the film morphology of the active layer by using the solvent vapor annealing method (here is CH_2Cl_2 for 30 s or 50 s), without the need of incorporation of an additive. It was found that the PCEs of the device at a 1:2/1:3 ratio of **BIT-4F-T:**PC$_{71}$BM were further enhanced to some extent. For example, a best PCE of 8.1% (J_{sc} = 11.9 mA cm^{-2}, V_{oc} = 0.90 V, *FF* = 76%) and an average PCE of 7.6% accounted over 30 individual devices were obtained for **BIT-4F-T:PC$_{71}$BM** (1:2) after CH_2Cl_2 vapor annealing for 30 s, which is particularly noteworthy given that the initial performance as well as very-high *FF* ranks one of the best reported in the literature. It is worthy to mention that longer annealing time (i.e., 50 s) only leads to a moderate enhancement in all of the device parameters (see Table 2), resulting in a best PCE of 7.4%. **Figure 4** shows the current density versus voltage (*J*–*V*) characteristics of the best device from **BIT-4F-T:PC$_{71}$BM (1:2)** before and after solvent vapor annealing. For comparison, the best *J*–*V* characteristics of other devices from other donors are also shown. Our novel and systematic work makes difluorinated benzothiadiazole and IDT-based small molecules become another novel, high-efficiency (>8% PCE vs the best 5.3% PCE based on IDT-small molecules from the literature,[8g] solution-processed, small-molecule donor materials after the previously reported BDT and DTS-based compounds.

To determine the origin of the observed photovoltaic performance differences between **BIT**, **BIT-4F**, and **BIT-4F-T** as well as the effect of solvent vapor annealing on the active layer, we carried out more detailed investigations into absorption properties, external quantum efficiency (EQE), their charge mobility, and morphology of blend films by atomic force microscopy (AFM) to draw a structure–property relationship.

To further understand the device performance, the EQE spectra of such device are measured and shown in Figure 4. All the EQE spectra covered a broad wavelength range from 300 to 750 nm and showed a maximum EQE value of 37% at 570 nm,

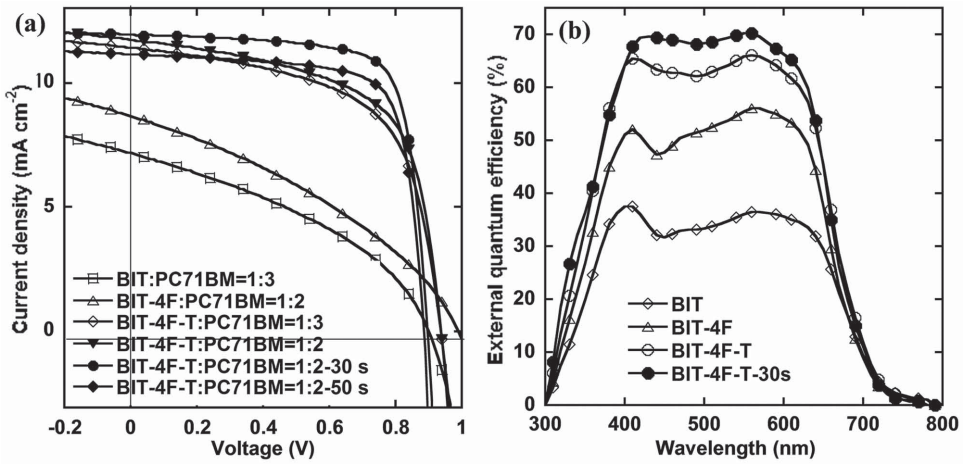

Figure 4. a) Current density–voltage (*J–V*) characteristics of the best OSC devices based on these D_1-A-D_2-A-D_1 small molecules and **$PC_{71}BM$** (different blend ratios and before/after CH_2Cl_2 vapor annealing). b) EQE plots of these materials with **$PC_{71}BM$** in a 1:2 blend ratio and before/after CH_2Cl_2 vapor annealing.

56% at 570 nm, 66% at 560 nm, and 70% at 560 nm for these devices based on **BIT:$PC_{71}BM$** (1:2), **BIT-4F:$PC_{71}BM$** (1:2), and **BIT-4F-T:$PC_{71}BM$** (1:2) before/after solvent treatment, respectively. Obviously, for a device with CH_2Cl_2 vapor annealing, the EQE was increased across the range of 400–600 nm, which indicated that the photo-electron conversion is highly efficient. The calculated J_{sc} values obtained by integration of the EQE data for these devices showed 2%–5% mismatch compared with the J_{sc} value from the *J–V* curve.

As shown in Figure 3, the intensity of absorption spectra of the active layer based on **BIT-4F-T** and **$PC_{71}BM$** was further enhanced upon CH_2Cl_2 vapor annealing, with well-defined features, i.e., 0–0 vibrational shoulder peak in the range of 600–650 nm, which is related to the enhanced π–π stacking and interaction of intermolecules by the increase in molecular planarity between difluorinated benzothiadiazole and IDT units. The observed substantial improvement in J_{sc} upon solvent vapor annealing can mainly be attributed to enhanced absorption. The results are consistent with the trend of the above EQE results.

On the other side, the morphology of blend film was found to be affected during CH_2Cl_2 vapor annealing, as revealed by the AFM. For the pristine film without any treatment, very smooth surface and uniform morphology with small roughness (<0.5 nm) and low phase domain (<10 nm) was observed (**Figure 5**a, Figure S6, Supporting Information), indicating that all of the donor materials have a good miscibility with $PC_{71}BM$. After CH_2Cl_2 vapor annealing for 30 s, the surface of the film based on the 1:2 ratio of **BIT-4F-T:$PC_{71}BM$** becomes slightly rougher with RMS roughness of 1.15 nm and coarse domain features (20–50 nm), and thus can form a well-interpenetrating network with clear donor–acceptor phase separation, which is consistent with the feature of the optical properties of the blend films upon CH_2Cl_2 vapor annealing. Obviously, the solvent vapor annealing provided a driving force to facilitate domain grow, resulting in the more obvious phase segregation between the donor/acceptor, and the more ordered film morphology of the active layer in nanoscale, which was in good agreement with the previous literature.[17] We guess that the improved morphologies of blend films are

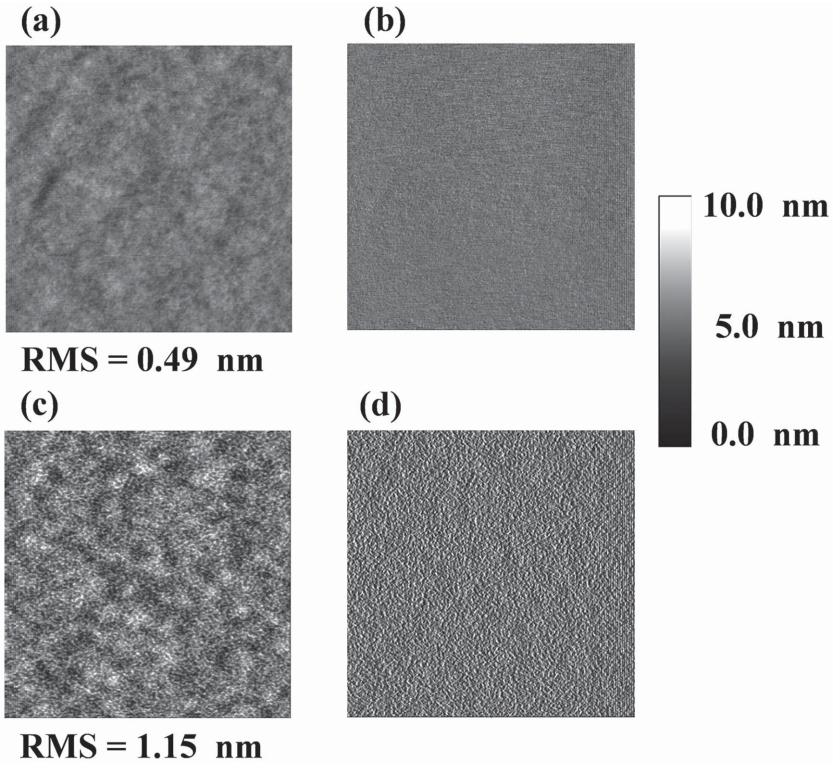

Figure 5. Tapping-mode a,c) AFM height and b,d) phase images 5 × 5 μm^2 of **BIT-4F-T/$PC_{71}BM$** (1:2, w/w) a,b) without and c,d) with CH_2Cl_2 vapor annealing in 30 s.

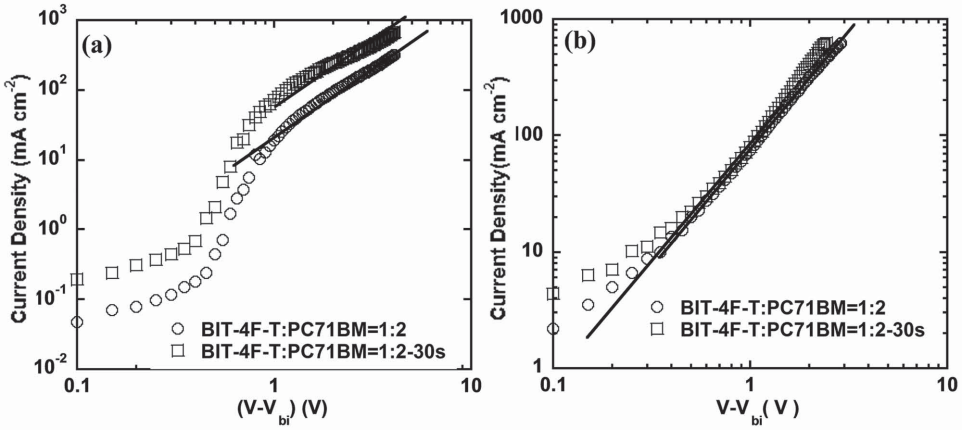

Figure 6. The *J–V* plots of the devices with a) a configuration of ITO/PEDOT/**BIT-4F-T**:$PC_{71}BM$ (1:2)/Au for a hole-only device and b) a configuration of ITO/ZnO/PFN/**BIT-4F-T**:$PC_{71}BM$ (1:2)/Ca/Al for an electron-only device. The open squares and circles are for the device before and after CH_2Cl_2 vapor annealing, respectively. The solid lines represent the best fitting from the space-charge-limited-current model.

preferable to improve charge transport properties upon CH_2Cl_2 vapor annealing as discussed below.[18]

To verify the positive effect of the solvent vapor annealing on charge transporting, we compared the hole and electron mobility in the actual device based on **BIT-4F-T** and $PC_{71}BM$ (1:2) before and after this treatment using a space charge limited current (SCLC) method. The structures of hole-only and electron-only device are ITO/PEDOT/**BIT-4F-T**:$PC_{71}BM$ (1:2)/MoO_3/Al and ITO/ZnO/PFN/**BIT-4F-T**:$PC_{71}BM$ (1:2)/Ca/Al, respectively. The hole and electron mobilities were obtained through space charge limited current (SCLC) method and **Figure 6** displays the *J–V* characteristics of the hole-only and electron-only devices as obtained in dark. The hole mobility for a device fabricated from **BIT-4F-T** is 7.3×10^{-5} cm^2 V^{-1} s^{-1}, while it was enhanced to 2.4×10^{-4} cm^2 V^{-1} s^{-1} after treatment with CH_2Cl_2 for 30 s, which corresponds to a threefold enhancement. Meanwhile, the electron mobility was slightly increased from 3.3×10^{-4} cm^2 V^{-1} s^{-1} to 3.5×10^{-4} cm^2 V^{-1} s^{-1} after CH_2Cl_2 vapor annealing for 30 s. The enhancement of charge carrier mobilities is consistent with the increase of R_{rms} in an AFM image. Moreover, the charge carrier ratio between electron and hole (μ_e/μ_h) is about 1.5 for device based on **BIT-4F-T**:$PC_{71}BM$ (1:2) after CH_2Cl_2 vapor annealing for 30 s, which represents a dramatic improvement when compared with that of the corresponding device without CH_2Cl_2 vapor annealing ($\mu_e/\mu_h \approx 4.5$). As the accumulation of space charges and recombination of charge carriers are processes that are closely related to the carrier mobilities of electron and hole, and the ratio between them,[19] we conclude that CH_2Cl_2 vapor annealing is very beneficial to the higher *FF* (up to 76%) and is responsible for the improvement in J_{sc} and overall performance.

3. Conclusion

In conclusion, a family of multifluorine substituted wide band gap small molecules with D_1-A-D_2-A-D_1 linear framework based on IDT and difluorobenzothiadiazole has been synthesized for BHJ-OSCs. Notably, a high PCE of 8.1% with the high V_{oc} (≈0.9 eV) and very high FF (≈0.76) for **BIT-4F-T** was achieved in a simple device configuration without an additional additive, which is among one of the highest reported for small-molecules-based solar cells that have only a few small molecules with PCE over 8%. This exciting result verifies that multiple fluorine substituents of benzothiadiazole and IDT flanked with two thiophene moieties are important toward high PCE. Compared with that of **BIT-4F**, inserting thiophene moieties can enhance the absorption intensity in the region of shorter wavelength (400–600 nm) and increase the vibrational feature significantly. Combined with multiple fluorine substituents of benzothiadiazole, **BIT-4F-T** can keep the relative lower HOMO energy level and improve the charge transport and PCE in comparison with **BIT**. The influence of solvent vapor annealing on the morphology of the photoactive layers was investigated by absorption spectra and AFM. Exposure to CH_2Cl_2 vapor allows for a reorganization of the blend to more ordered and favorable film morphology, which further increased the intensity and vibrational feature of absorption, improved the balance of charge carrier mobility, phase domain features, and PCE. The results reported here also clearly indicate that high PCE in solar cell based small molecules be significantly increased through careful engineering of the molecular structure and optimization of the morphology of blend films to enhance the intermolecular interactions. We also note that with the high V_{oc} (≈0.9 eV) and very high FF (≈0.76), **BIT-4F-T** can find applications in tandem solar cells as a promising key component.

4. Experimental Section

Materials and Characterization: All air and water-sensitive reactions were performed under nitrogen atmosphere. Tetrahydrofuran (THF) was dried over Na/benzophenone ketyl and freshly distilled prior to use. The other materials were of the common commercial level and used as received. Thin layer chromatography (TLC) was conducted on flexible sheets precoated with SiO_2 and the separated products were visualized by UV light. Column chromatography was conducted using SiO_2 (300 mesh) from Fisher Scientific. ^1H and ^{13}C NMR spectra were recorded on a Bruker ARX-400 (400 MHz) or ARX-500 (500 MHz) spectrometer, using $CDCl_3$, except where noted. All chemical shifts

were reported in parts per million (ppm). ^{1}H NMR chemical shifts were referenced to $CDCl_3$ (7.26 ppm), and ^{13}C NMR chemical shifts were referenced to $CDCl_3$ (77.23 ppm). MALDI-TOF-MS was recorded on a Bruker BIFLEX III mass spectrometer. Thermal gravity analyses (TGA) were carried out on a TA Instrument Q600 analyzer. Elemental analyses were performed using a German Vario EL III elemental analyzer. Absorption spectra were recorded on PerkinElmer Lambda 750 UV–vis spectrometer. CV was performed on BASI Epsilon workstation. Glassy carbon electrode was used as a working electrode and a platinum wire as a counter electrode. These films were drop cast on a glass carbon working electrode from THF at a concentration of 5 mg mL^{-1}. Measurements were carried out at a scan rate of 50 mV s^{-1} in CH_3CN containing 0.1 M n-Bu_4NPF_6 as the supporting electrolyte. All potentials were recorded versus Ag/AgCl reference electrode and calibrated with the redox couple of Fc/Fc^+ under the same experimental conditions.

BHJ-OSC Fabrication: Device preparation and characterization were carried out under clean room conditions with protection against dust and moisture. The fabrication of OSCs followed the procedures described in our previous paper.[14]

Characterization and Measurement: The values of power conversion efficiency were determined from *J–V* characteristics measured by a Keithley 2400 source-measurement unit under AM 1.5G spectrum from a solar simulator (Oriel model 91192). Masks made from laser beam cutting technology with a well-defined area of 16.0 mm^2 were attached to define the effective area for accurate measurement. Solar simulator illumination intensity was determined using a monocrystal silicon reference cell (Hamamatsu S1133, with KG-5 visible color filter) calibrated by the National Renewable Energy Laboratory (NREL). The active layer was spin coated from blend chloroform solutions with a weight ratio of **BIT-4F-T** and $PC_{71}BM$ at 1:2 (or other ratios) and then was placed in a glass petri dish containing 1 mL CH_2Cl_2 for 30 s or 50 s for solvent vapor annealing. The film morphology was studied by AFM (Veeco MultiMode V) operating in tapping mode. EQE values of the encapsulated devices were measured by using an integrated system (Enlitech, Taiwan, China) and a lock-in amplifier with a current preamplifier under short-circuit conditions. The devices were illuminated by monochromatic light from a 75 W xenon lamp. The light intensity was determined by using a calibrated silicon photodiode.

BIT-4F: To a 100 mL two-neck round-bottom flask, **3** (210 mg, 0.20 mmol), **8** (250 mg, 0.50 mmol), $Pd_2(dba)_3$ (9.1 mg, 0.01 mmol), and tri(*o*-tolyl) phosphine (12.4 mg, 0.04 mmol) were added. The flask was evacuated and back-filled with N_2 three times, and then degassed toluene was injected into the mixture. The resulting solution was stirred at refluxing temperature for 12 h under the N_2 atmosphere. After being cooled to room temperature, the solvents were then removed under reduced pressure. The dark residue was purified by silica gel chromatography, eluting with PE-CH_2Cl_2 (10:1) to give dark solid (265 mg, 86%). ^{1}H NMR ($CDCl_3$, 400 MHz, ppm): δ 8.24–8.32 (m, 2H, Th-H), 8.19–8.21 (m, 2H, Th-H), 7.52 (s, 2H, Ph-H), 7.23–7.24 (d, J = 3.6 Hz, 2H, Th-H), 7.15–7.16 (d, J = 3.6 Hz, 2H, Th-H), 6.74–6.75 (d, J = 3.6 Hz, 1H, Th-H), 2.81–2.85 (m, 4H, CH_2), 2.10–2.13 (m, 8H, CH_2), 1.70–1.74 (m, 4H, CH_2), 1.26–1.43 (m, 12H, CH_2), 0.89–0.98 (m, 40H, CH_2, CH_3), 0.56–0.73 (m, 26H, CH_2, CH_3). ^{13}C NMR ($CDCl_3$, 100 MHz, ppm): δ 155.7, 154.0, (149.1, 149.0), 146.7, (141.5, 141.4), 136.5, 134.5, 133.3, (131.9, 131.8), 130.3, 126.6, 125.3, 124.3, 123.5, 115.0, 112.7, (111.0, 110.9), 54.3, (44.4, 43.9), (35.3, 35.2), (34.4, 34.3, 34.2), (31.80, 31.78), 30.5, (29.0, 28.8, 28.7, 28.5), (28.49, 28.44), (27.5, 27.4), (23.11, 23.08, 23.0, 22.8), (14.4, 14.3, 14.2), (10.9, 10.8, 10.6, 10.5). MALDI-TOF MS (m/z): calcd for $C_{88}H_{106}F_4N_4S_8$: 1550.6. Found: 1550.7 (M^+). Elemental Analysis: calcd for $C_{88}H_{106}F_4N_4S_8$: C, 68.09; H, 6.88; N, 3.61. Found: C, 68.02; H, 6.87; N, 3.55.

BIT-4F-T: To a 100 mL two-neck round-bottom flask, **5** (0.44 g, 0.36 mmol), **8** (0.45 g, 0.90 mmol), $Pd_2(dba)_3$ (35 mg, 0.04 mmol), and tri(*o*-tolyl) phosphine (50 mg, 0.16 mmol) were added. The flask was evacuated and back-filled with N_2 three times, and then degassed toluene was injected into the mixture. The resulting solution was stirred at refluxing temperature for 12 h under the N_2 atmosphere. After being cooled to room temperature, the solvents were then removed under reduced pressure. The dark residue was purified by silica gel chromatography, eluting with PE-$CHCl_3$ (5:1) to give dark solid (380 mg, 61%). ^{1}H NMR ($CDCl_3$, 400 MHz, ppm): δ 8.23–8.24 (m, 2H, Th-H), 8.19–8.21 (d, J = 3.6 Hz, 2H, Th-H), 7.33 (m, 4H, Ph-H, Th-H), 7.28 (m, 2H, Th-H), 7.23–7.24 (d, J = 3.6 Hz, 2H, Th-H), 7.15–7.16 (d, J = 3.6 Hz, 2H, Th-H), 6.73–6.74 (d, J = 3.6 Hz, 1H, Th-H), 2.81–2.85 (t, J = 7.6 Hz, 4H, CH_2), 2.01 (m, 8H, CH_2), 1.70–1.73 (m, 4H, CH_2), 1.33–1.43 (m, 12H, CH_2), 0.89–1.04 (m, 40H, CH_2, CH_3), 0.55–0.77 (m, 26H, CH_2, CH_3). ^{13}C NMR ($CDCl_3$, 100 MHz, ppm): δ 156.2, 153.3, (151.0, 150.9), (149.0, 148.9), 148.8, 146.8, 142.4, (141.7, 141.6), 138.1, 136.0, 134.5, (132.2, 132.1, 132.04, 131.97), 130.1, 125.3, 124.4, (123.5, 123.4), 120.1, 114.3, 111.4, 54.3, (44.4, 43.9), (35.32, 35.28), (34.6, 34.5), (34.2, 34.0), (31.81, 31.77), 30.5, (29.01, 28.89), 28.5, (27.7, 27.54, 27.46, 27.3), (23.2, 23.13, 23.08), 22.8, (14.4, 14.34, 14.3), (11.0, 10.9, 10.62, 10.56). MALDI-TOF MS (m/z): calcd for $C_{96}H_{110}F_4N_4S_{10}$: 1714.6. Found: 1714.2 (M^+). Elemental Analysis: calcd for $C_{96}H_{110}F_4N_4S_{10}$: C, 67.17; H, 6.46; N, 3.26. Found: C, 66.94; H, 6.38; N, 3.22.

BIT: To a 100 mL two-neck round-bottom flask, **3** (210 mg, 0.20 mmol), **9** (232 mg, 0.50 mmol), $Pd_2(dba)_3$ (9.1 mg, 0.01 mmol), and tri(*o*-tolyl) phosphine (12.4 mg, 0.04 mmol) were added. The flask was evacuated and back-filled with N_2 three times, and then degassed toluene was injected into the mixture. The resulting solution was stirred at refluxing temperature for 12 h under the N_2 atmosphere. After being cooled to room temperature, the solvents were then removed under reduced pressure. The dark residue was purified by silica gel chromatography, eluting with PE-CH_2Cl_2 (20:1) to give dark solid (265 mg, 91%). ^{1}H NMR ($CDCl_3$, 400 MHz, ppm): δ 8.09–8.17 (m, 2H, Th-H), 8.04–8.05 (m, 2H, Th-H), 7.84–7.91 (d, d, J = 7.6 Hz, 4H, Ph-H), 7.43 (s, 2H, Ph-H), 7.20–7.21 (d, J = 3.6 Hz, 2H, Th-H), 7.11–7.12 (d, J = 3.6 Hz, 2H, Th-H), 6.73–6.74 (d, J = 3.6 Hz, 2H, Th-H), 2.81–2.85 (t, J = 7.6 Hz, 4H, CH_2), 2.07–2.11 (m, 8H, CH_2), 1.68–1.75 (m, 4H, CH_2), 1.33–1.43 (m, 12H, CH_2), 0.90–0.98 (m, 40H, CH_2, CH_3), 0.54–0.72 (m, 26H, CH_2, CH_3). ^{13}C NMR ($CDCl_3$, 100 MHz, ppm): δ (156.23, 156.18), 153.5, 152.8, 152.7, 146.1, (144.15, 144.11, 144.06), 140.9, 139.3, 137.8, 136.4, 134.9, 128.2, 126.9, 125.3, 125.2, 125.1, 124.5, 124.0, 123.9, (125.5, 123.3, 123.2), 114.6, (54.28, 54.25), (44.3, 43.9), (35.24, 35.21), (34.5, 34.4), (34.2, 34.1), (31.79, 31.77), 30.5, (29.0, 28.9, 28.7, 28.5, 28.4), (27.6, 27.4), (23.1, 23.0, 22.8), (14.4, 14.31, 14.28), (11.0, 10.8, 10.7, 10.62, 10.59). MALDI-TOF MS (m/z): calcd for $C_{88}H_{110}N_4S_8$: 1478.7. Found: 1478.8 (M^+). Elemental Analysis: calcd for $C_{88}H_{110}N_4S_8$: C, 71.40; H, 7.49; N, 3.78. Found: C, 71.16; H, 7.33; N, 3.74.

Supporting Information

Supporting Information is available from the Wiley Online Library or from the author.

Acknowledgements

J.-L.W., Q.-R.Y., and J.-S.M. contributed equally to this work. This work was financially supported by the grants from the National Natural Science Foundation of China (21202007, 21472012, 51225301, 91333206), the Thousand Youth Talents Plan of China, Beijing Natural Science Foundation (2152027), the Development Program for Distinguished Young and Middle-Aged Teachers and Special programs to cultivate major projects of the Beijing Institute of Technology.

Received: January 16, 2015
Revised: March 11, 2015
Published online: May 4, 2015

[1] a) G. Dennler, M. C. Scharber, C. J. Brabec, *Adv. Mater.* **2009**, *21*, 1323; b) H.-Y. Chen, J. Hou, S. Zhang, Y. Liang, G. Yang, Y. Yang,

L. Yu, Y. Wu, G. Li, *Nat. Photonics* **2009**, *3*, 649; c) O. Inganäs, F. Zhang, M. R. Andersson, *Acc. Chem. Res.* **2009**, *42*, 1731; d) T.-Y. Chu, J. Lu, S. Beaupré, Y. Zhang, J.-R. Pouliot, S. Wakim, J. Zhou, M. Leclerc, Z. Li, J. Ding, Y. Tao, *J. Am. Chem. Soc.* **2011**, *133*, 4250; e) M. Wang, X. Hu, P. Liu, W. Li, X. Gong, F. Huang, Y. Cao, *J. Am. Chem. Soc.* **2011**, *133*, 9638; f) P. M. Beaujuge, J. M. J. Fréchet, *J. Am. Chem. Soc.* **2011**, *133*, 20009; g) Y. Li, *Acc. Chem. Res.* **2012**, *45*, 723; h) H. Zhou, L. Yang, W. You, *Macromolecules* **2012**, *45*, 607; i) C. Cabanetos, A. E. Labban, J. A. Bartelt, J. D. Douglas, W. R. Mateker, J. M. J. Fréchet, M. D. McGehee, P. M. Beaujuge, *J. Am. Chem. Soc.* **2013**, *135*, 4656; j) K. Li, Z. Li, K. Feng, X. Xu, L. Wang, Q. Peng, *J. Am. Chem. Soc.* **2013**, *135*, 13549; k) I. Osaka, T. Kakara, N. Takemura, T. Koganezawa, K. Takimiya, *J. Am. Chem. Soc.* **2013**, *135*, 8834; l) K. H. Hendriks, G. H. L. Heintges, V. S. Gevaerts, M. M. Wienk, R. A. J. Janssen, *Angew. Chem. Int. Ed.* **2013**, *52*, 8341; m) L. Ye, S. Zhang, L. Huo, M. Zhang, J. Hou, *Acc. Chem. Res.* **2014**, *47*, 1595; n) T. Qin, W. Zajaczkowski, W. Pisula, M. Baumgarten, M. Chen, M. Gao, G. Wilson, C. D. Easton, K. Müllen, S. E. Watkins, *J. Am. Chem. Soc.* **2014**, *136*, 6049.

[2] a) Z. He, C. Zhong, S. Su, M. Xu, H. Wu, Y. Cao, *Nat. Photon.* **2012**, *6*, 593; b) J.-D. Chen, C. Cui, Y.-Q. Li, L. Zhou, Q.-D. Ou, C. Li, Y. Li, J.-X. Tang, *Adv. Mater.* **2015**, *27*, 10135; c) Y. Liu, J. Zhao, Z. Li, C. Mu, W. Ma, H. Hu, K. Jiang, H. Lin, H. Ade, H. Yan, *Nat. Commun.* **2014**, *5*, 5293; d) L. Ye, S. Zhang, W. Zhao, H. Yao, J. Hou, *Chem. Mater.* **2014**, *26*, 3603; e) T. L. Nguyen, H. Choi, S.-J. Ko, M. A. Uddin, B. Walker, S. Yum, J.-E. Jeong, M. H. Yun, T. J. Shin, S. Hwang, J. Y. Kim, H. Y. Woo, *Energy Environ. Sci.* **2014**, *7*, 3040; f) C.-C. Chen, W.-H. Chang, K. Yoshimura, K. Ohya, J. You, J. Gao, Z. Hong, Y. Yang, *Adv. Mater.* **2014**, *26*, 5670.

[3] a) C. Li, M. Liu, N. G. Pschirer, M. Baumgarten, K. Müllen, *Chem. Rev.* **2010**, *110*, 6817; b) B. Walker, C. Kim, T.-Q. Nguyen, *Chem. Mater.* **2011**, *23*, 470; c) A. Mishra, P. Bäuerle, *Angew. Chem. Int. Ed.* **2012**, *51*, 2020; d) Y. Lin, Y. Li, X. Zhan, *Chem. Soc. Rev.* **2012**, *41*, 4245; e) Y. Chen, X. Wan, G. Long, *Acc. Chem. Res.* **2013**, *46*, 2645; f) J. E. Coughlin, Z. B. Henson, G. C. Welch, G. C. Bazan, *Acc. Chem. Res.* **2014**, *47*, 257; g) J. Roncali, P. Leriche, P. Blanchard, *Adv. Mater.* **2014**, *26*, 3821.

[4] a) B. Walker, A. B. Tamayo, X.-D. Dang, P. Zalar, J. H. Seo, A. Garcia, M. Tantiwiwat, T.-Q. Nguyen, *Adv. Funct. Mater.* **2009**, *19*, 3063; b) L. Bu, X. Guo, B. Yu, Y. Qu, Z. Xie, D. Yan, Y. Geng, F. Wang, *J. Am. Chem. Soc.* **2009**, *131*, 13242; c) M. Seri, A. Marrocchi, D. Bagnis, R. Ponce, A. Taticchi, T. J. Marks, A. Facchetti, *Adv. Mater.* **2011**, *23*, 3827; d) H. Shang, H. Fan, Y. Liu, W. Hu, Y. Li, X. Zhan, *Adv. Mater.* **2011**, *23*, 1554; e) T. Bura, N. Leclerc, S. Fall, R. Lévêque, T. Heiser, P. Retailleau, S. Rihn, A. Mirloup, R. Ziessel, *J. Am. Chem. Soc.* **2012**, *134*, 17404; f) H. Bürckstummer, E. V. Tulyakova, M. Deppisch, M. R. Lenze, N. M. Kronenberg, M. Gsänger, M. Stolte, K. Meerholz, F. Würthner, *Angew. Chem. Int. Ed.* **2011**, *50*, 11628; g) X. Xiao, G. Wei, S. Wang, J. D. Zimmerman, C. K. Renshaw, M. E. Thompson, S. R. Forrest, *Adv. Mater.* **2012**, *24*, 1956; h) S. Shen, P. Jiang, C. He, J. Zhang, P. Shen, Y. Zhang, Y. Yi, Z. Zhang, Z. Li, Y. Li, *Chem. Mater.* **2013**, *25*, 2274; i) J. Huang, C. Zhan, X. Zhang, Y. Zhao, Z. Lu, H. Jia, B. Jiang, J. Ye, S. Zhang, A. Y. Tang, Liu, Q. Pei, J. Yao, *ACS Appl. Mater. Interfaces* **2013**, *5*, 2033; j) A. Sharenko, C. M. Proctor, T. S. van der Poll, Z. B. Henson, T.-Q. Nguyen, G. C. Bazan, *Adv. Mater.* **2013**, *25*, 4403; k) J. Liu, Y. Sun, P. Moonsin, M. Kuik, C. M. Proctor, J. Lin, B. B. Hsu, V. Promarak, A. J. Heeger, T.-Q. Nguyen, *Adv. Mater.* **2013**, *25*, 5898; l) Y. S. Park, T. S. Kale, C.-Y. Nam, D. Choi, R. B. Grubbs, *Chem. Commun.* **2014**, *50*, 7964; m) H. Qin, L. Li, F. Guo, S. Su, J. Peng, Y. Cao, X. Peng, *Energy Environ. Sci.* **2014**, *7*, 1397; n) C. Yu, Z. Liu, Y. Yang, J. Yao, Z. Cai, H. Luo, G. Zhang, D. Zhang, *J. Mater. Chem. C* **2014**, *2*, 10101; o) Y. R. Cheon, Y. J. Kim, J. Y. Back, T. K. An, C. E. Park, Y.-H. Kim, *J. Mater. Chem. A* **2014**, *2*, 16443; p) D. Liu, M. Xiao, Z. Du, Y. Yan, L. Han, V. A. L. Roy, M. Sun, W. Zhu, C. S. Lee, R. Yang, *J. Mater. Chem. A* **2014**, *2*, 7523; q) N. Lim, N. Cho, S. Paek, C. Kim, J. K. Lee, J. Ko, *Chem. Mater.* **2014**, *26*, 2283; r) H. Gao, Y. Li, L. Wang, C. Ji, Y. Wang, W. Tian, X. Yang, L. Yin, *Chem. Commun.* **2014**, *50*, 10251; s) W. Shin, T. Yasuda, Y. Hidaka, G. Watanabe, R. Arai, K. Nasu, T. Yamaguchi, W. Murakami, K. Makita, C. Adachi, *Adv. Energy. Mater.* **2014**, 1400879.

[5] a) Y. Liu, X. Wan, F. Wang, J. Zhou, G. Long, J. Tian, Y. Chen, *Adv. Mater.* **2011**, *23*, 5387; b) Z. Li, G. He, X. Wan, Y. Liu, J. Zhou, G. Long, Y. Zuo, M. Zhang, Y. Chen, *Adv. Energy. Mater.* **2012**, *2*, 74; c) J. Zhou, X. Wan, Y. Liu, Y. Zuo, Z. Li, G. He, G. Long, W. Ni, C. Li, X. Su, Y. Chen, *J. Am. Chem. Soc.* **2012**, *134*, 16345; d) J. Zhou, Y. Zuo, X. Wan, G. Long, Q. Zhang, W. Ni, Y. Liu, Z. Li, G. He, C. Li, B. Kan, M. Li, Y. Chen, *J. Am. Chem. Soc.* **2013**, *135*, 8484; e) Y. Liu, C.-C. Chen, Z. Hong, J. Gao, Y. Yang, H. Zhou, L. Dou, G. Li, Y. Yang, *Sci. Rep.* **2013**, *3*, 3356; f) B. Kan, Q. Zhang, M. Li, X. Wan, W. Ni, G. Long, Y. Wang, X. Yang, H. Feng, Y. Chen, *J. Am. Chem. Soc.* **2014**, *136*, 15529.

[6] a) Y. Sun, G. C. Welch, W. L. Leong, C. J. Takacs, G. C. Bazan, A. J. Heeger, *Nat. Mater.* **2012**, *11*, 44; b) C. Takacs, Y. Sun, G. Welch, L. A. Perez, X. Liu, W. Wen, G. C. Bazan, A. J. Heeger, *J. Am. Chem. Soc.* **2012**, *134*, 16597; c) T. S. van der Poll, J. A. Love, T.-Q. Nguyen, G. C. Bazan, *Adv. Mater.* **2012**, *24*, 3646; d) D. H. Wang, A. K. K. Kyaw, V. Gupta, G. C. Bazan, A. J. Heeger, *Adv. Energy Mater.* **2013**, 1161; e) V. Gupta, A. Kyaw, K. K. D. H. Wang, S. Chand, G. C. Bazan, A. J. Heeger, *Sci. Rep.* **2013**, *3*, 1965; f) A. K. K. Kyaw, D. H. Wang, D. Wynands, J. Zhang, T.-Q. Nguyen, G. C. Bazan, A. J. Heeger, *Nano Lett.* **2013**, *13*, 3796; g) J. A. Love, I. Nagao, Y. Huang, M. Kuik, V. Gupta, C. J. Takacs, J. E. Coughlin, L. Qi, T. S. van der Poll, E. J. Kramer, A. J. Heeger, T.-Q. Nguyen, G. C. Bazan, *J. Am. Chem. Soc.* **2014**, *136*, 3597; h) X. Liu, Y. Sun, B. B. Y. Hsu, A. Lorbach, L. Qi, A. J. Heeger, G. C. Bazan, *J. Am. Chem. Soc.* **2014**, *136*, 5697; i) Y. Sun, J. Seifter, L. Huo, Y. Yang, B. B. Y. Hsu, H. Zhou, X. Sun, S. Xiao, L. Jiang, A. J. Heeger, *Adv. Energy Mater.* **2014**, 1400987.

[7] a) S. Albrecht, S. Janitz, W. Schindler, J. Frisch, J. Kurpiers, J. Kniepert, S. Inal, P. Pingel, K. Fostiropoulos, N. Koch, D. Neher, A. C. Stuart, *J. Am. Chem. Soc.* **2012**, *134*, 14932; b) J. R. Tumbleston, H. Zhou, W. Li, S. Liu, H. Ade, W. You, *J. Am. Chem. Soc.* **2013**, *135*, 1806; c) N. Wang, Z. Chen, W. Wei, Z. Jiang, *J. Am. Chem. Soc.* **2013**, *135*, 17060; d) J. H. Park, E. H. Jung, J. W. Jung, W. H. Jo, *Adv. Mater.* **2013**, *25*, 2583; e) S. Yum, T. K. An, X. Wang, W. Lee, M. A. Uddin, Y. J. Kim, T. L. Xu, S. Nguyen, S. Hwang, C. E. Park, H. Y. Woo, *Chem. Mater.* **2014**, *26*, 2147; f) M. Zhang, X. Guo, S. Zhang, J. Hou, *Adv. Mater.* **2014**, *26*, 1118.

[8] a) M. Zhang, X. Guo, X. Wang, H. Wang, Y. Li, *Chem. Mater.* **2011**, *23*, 4264; b) R. S. Ashraf, B. C. Schroeder, H. A. Bronstein, Z. Huang, S. Thomas, R. J. Kline, C. J. Brabec, P. Rannou, T. D. Anthopoulos, J. R. Durrant, I. McCulloch, *Adv. Mater.* **2013**, *25*, 2029; c) J. J. Intemann, K. Yao, H.-L. Yip, Y.-X. Xu, Y.-X. Li, P.-W. Liang, F.-Z. Ding, X. Li, A. K.-Y. Jen, *Chem. Mater.* **2013**, *25*, 3188; d) H. Bronstein, J. M. Frost, A. Hadipour, Y. Kim, C. B. Nielsen, R. S. Ashraf, B. P. Rand, S. Watkins, I. McCulloch, *Chem. Mater.* **2013**, *25*, 277; e) W. Yong, M. Zhang, X. Xin, Z. Li, Y. Wu, X. Guo, Z. Yang, J. Hou, *J. Mater. Chem. A* **2013**, *1*, 14214; f) X. Liu, Q. Li, Y. Li, X. Gong, S.-J. Su, Y. Cao, *J. Mater. Chem. A* **2014**, *2*, 4004; g) H. Bai, Y. Wang, P. Cheng, Y. Li, D. Zhu, X. Zhan, *ACS Appl. Mater. Interfaces* **2014**, *6*, 8426.

[9] a) X. Wang, H. Luo, Y. Sun, M. Zhang, X. Li, G. Yu, Y. Liu, Y. Li, H. Wang, *J. Polym. Sci., Part A: Polym. Chem.* **2012**, *50*, 371; b) L. Cai, T. Moehl, S.-J. Moon, J.-D. Decoppet, R. Humphry-Baker, Z. Xue, L. Bin, S. M. Zakeeruddin, M. Grätzel, *Org. Lett.* **2014**, *16*, 106.

[10] C. Zhao, Y. Zhang, M.-K. Ng, *J. Org. Chem.* **2007**, *72*, 6364.

[11] L. Dou, C.-C. Chen, Y. Yoshimura, K. Ohya, W.-H. Chang, J. Gao, Y. Liu, E. Richard, Y. Yang, *Macromolecules* **2013**, *46*, 3384.
[12] M. Melucci, L. Favaretto, A. Zanelli, M. Cavallini, A. Bongini, P. Maccagnani, P. Ostoja, G. Derue, R. Lazzaroni, G. Barbarella, *Adv. Funct. Mater.* **2010**, *20*, 445.
[13] a) M. Zhang, X. Guo, W. Ma, S. Zhang, L. Huo, H. Ade, J. Hou, *Adv. Mater.* **2013**, *26*, 2089; b) T. L. Nguyen, H. Choi, S.-J. Ko, M. A. Uddin, B. Walker, S. Yum, J.-E. Jeong, M. H. Yun, T. J. Shin, S. Hwang, J. Y. Kim, H. Y. Woo, *Energy Environ. Sci.* **2014**, *7*, 3040.
[14] M. J. Frisch, G. W. Trucks, H. B. Schlegel, G. E. Scuseria, M. A. Robb, J. R. Cheeseman, G. Scalmani, V. Barone, B. Mennucci, G. A. Petersson, H. Nakatsuji, M. Caricato,X. Li, H. P. Hratchian, A. F. Izmaylov, J. Bloino, G. Zheng, J. L. Sonnenberg, M. Hada, K. Toyota, R. Fukuda, J. Hasegaw, M. Ishida, T. Nakajima, Y. Honda, O. Kitao, H. Nakai, T. Vreven, J. A. Montgomery, J. E. Peralta, F. Ogliaro, M. Bearpark, J. J. Heyd, E. Brothers, K. N. Kudin, V. N. Staroverov, R. Kobayashi, J. Normand, K. Raghavachari, A. Rendell, J. C. Burant, S. S. Iyengar, J. Tomasi, M. Cossi, N. Rega, N. J. M. Millam, M. Klene, J. E. Knox, J. B. Cross, V. Bakken, C. Adamo, J. Jaramillo, R. Gomperts, R. E. Stratmann, O. Yazyev, A. J. Austin, R. Cammi, C. Pomelli, J. W. Ochterski, R. L. Martin, K. Morokuma, V. G. Zakrzewski, G. A. Voth, P. Salvador, J. J. Dannenberg, S. Dapprich, A. D. Daniels, Ö. Farkas, *Gaussian 09. Revision A.01*, Gaussian Inc., Wallingford, CT **2009**.
[15] Z. C. He, C. M. Zhong, X. Huang, W.-Y. Wong, H. B. Wu, L. W. Chen, S. J. Su, Y. Cao, *Adv. Mater.* **2011**, *23*, 4636.
[16] a) G. Li, Y. Yao, H. Yang, V. Shrotriya, G. Yang, Y. Yang, *Adv. Funct. Mater.* **2007**, *17*, 1636; b) J. G. Liu, L. Chen, B. R. Gao, X. X. Cao, Y. C. Han, Z. Y. Xie, L. X. Wang, *J. Mater. Chem. A* **2013**, *1*, 6216.
[17] G. Wei, S. Wang, K. Sun, M. E. Thompson, S. R. Forrest, *Adv. Energy Mater.* **2011**, *1*, 184.
[18] a) C. D. Wessendorf, G. L. Schulz, A. Mishra, P. Kar, I. Ata, M. Weidelener, M. Urdanpilleta, J. Hanisch, E. Mena-Osterita, M. Lindén, E. Ahlswede, P. Bäuerle, *Adv. Energy Mater.* **2014**, *4*, 1400266; b) K. Sun, Z. Xiao, E. Hanssen, M. F. G. Klein, H. H. Dam, M. Pfaff, D. Gerthsen, W. W. H. Wong, D. J. Jones, *J. Mater. Chem. A* **2014**, *2*, 9048.
[19] a) D. Patra, C.-C. Chiang, W.-A. Chen, K.-H. Wei, M.-C. Wu, C.-W. Chu, *J. Mater. Chem. A* **2013**, *1*, 7767; b) C. M. Proctor, J. A. Love, T.-Q. Nguyen, *Adv. Mater.* **2014**, *26*, 5957.